Dust radiative forcing in snow of the Upper Colorado River Basin: 1. A 6 year record of energy balance, radiation, and dust concentrations

Thomas H. Painter,[1,2,3] S. McKenzie Skiles,[2,3] Jeffrey S. Deems,[4,5] Ann C. Bryant,[6] and Christopher C. Landry[7]

Received 27 February 2012; revised 25 May 2012; accepted 7 June 2012; published 26 July 2012.

[1] Dust in snow accelerates snowmelt through its direct reduction of snow albedo and its further indirect reduction of albedo by accelerating the growth of snow grains. Since the westward expansion of the United States that began in the mid-19th century, the mountain snow cover of the Colorado River Basin has been subject to five-fold greater dust loading, largely from the Colorado Plateau and Great Basin. Radiative forcing of snowmelt by dust is not captured by conventional micrometeorological measurements, and must be monitored by a more comprehensive suite of radiation instruments. Here we present a 6 year record of energy balance and detailed radiation measurements in the Senator Beck Basin Study Area, San Juan Mountains, Colorado, USA. Data include broadband irradiance, filtered irradiance, broadband reflected flux, filtered reflected flux, broadband and visible albedo, longwave irradiance, wind speed, relative humidity, and air temperatures. The gradient of the snow surface is monitored weekly and used to correct albedo measurements for geometric effects. The snow is sampled weekly for dust concentrations in plots immediately adjacent to each tower over the melt season. Broadband albedo in the last weeks of snow cover ranged from 0.33 to 0.55 across the 6 years and two sites. Total end of year dust concentration in the top 3 cm of the snow column ranged from 0.23 mg g^{-1} to 4.16 mg g^{-1}. These measurements enable monitoring and modeling of dust and climate-driven snowmelt forcings in the Upper Colorado River Basin.

Citation: Painter, T. H., S. M. Skiles, J. S. Deems, A. C. Bryant, and C. C. Landry (2012), Dust radiative forcing in snow of the Upper Colorado River Basin: 1. A 6 year record of energy balance, radiation, and dust concentrations, *Water Resour. Res.*, *48*, W07521, doi:10.1029/2012WR011985.

1. Introduction

[2] The runoff from the Colorado River supplies water to over 30 million people in seven United States and Mexico. Climate change projections suggest that this runoff will decrease in the next 50 years by 7–20% due to increases in evapotranspiration and decreases in the ratio of snowfall to rain [*Christensen and Lettenmaier*, 2007; *Barnett and Pierce*, 2009]. Such scenarios challenge the sustainability of the freshwater supply to the southwest United States [*MacDonald*, 2010].

[3] Recent research however has shown that radiative forcing by dust in snow has been shortening snow cover duration by several weeks due to a 5–7-fold increase in dust loading since the period prior to the European-settlement of the western United States in the mid-1800s [*Painter et al.*, 2007; *Neff et al.*, 2008]. Extended to the scale of the Upper Colorado River Basin, this impact has brought peak normalized runoff at Lee's Ferry, Arizona (Lake Powell) more than three weeks earlier and reduced the total annual runoff by an average of ~5% [*Painter et al.*, 2010].

[4] Based on this new understanding of dust's influence on snow cover, water managers in the Upper Colorado basin now seek detailed real-time knowledge of dust presence, radiative forcing, and its potential to accelerate snowmelt, as well as understanding its implications for water supply under current conditions and in a changed climate. Likewise, water stakeholder groups, water conservation districts, and state and federal agencies are discussing efforts to restabilize soil surfaces in the dust-emitting regions to mitigate impacts of dust on snowmelt and runoff.

[5] Growing field observations and modeling simulations also suggest that increases in dust and black carbon deposition to snow in the Hindu Kush-Himalaya lead to retreat

[1]Jet Propulsion Laboratory, California Institute of Technology, Pasadena, California, USA.
[2]Department of Geography, University of California, Los Angeles, California, USA.
[3]Joint Institute for Regional Earth System Science and Engineering, University of California, Los Angeles, California, USA.
[4]National Snow and Ice Data Center, Boulder, Colorado, USA.
[5]NOAA Western Water Assessment, Boulder, Colorado, USA.
[6]Department of Geography, University of Utah, Salt Lake City, Utah, USA.
[7]Center for Snow and Avalanche Studies, Silverton, Colorado, USA.

Corresponding author: T. H. Painter, Jet Propulsion Laboratory, California Institute of Technology, 4800 Oak Grove Dr., Pasadena, CA 91109, USA. (thomas.painter@jpl.nasa.gov)

0043-1397/12/2012WR011985

and downwasting of glaciers [*Ramanathan et al.*, 2007; *Kaspari et al.*, 2009]. These results along with studies of the damaging health impacts of black carbon and other industrial pollutants have led to recent statements from the United Nations Environment Programme [*United Nations Environmental Programme/World Meteorological Organization*, 2011], the Vatican Pontifical Academy of Sciences [*Ajai et al.*, 2011], and the U.S. Department of State's initiation of the Climate and Clean Air Coalition to Reduce Short-Lived Climate Pollutants about the need to reduce atmospheric and cryosphere loading of carbonaceous particles. The studies that support these statements however have been performed without sustained in situ or remotely sensed observations of the variation of radiative forcing in snow, except for the present measurements.

[6] As these policy-related activities grow, it is imperative that we improve our understanding of the interannual variability of dust loading, the radiative forcing by dust, and the impacts on snowmelt. In 2003/2004, a collaboration between the lead author and coauthor Landry, Executive Director of the Center for Snow and Avalanche Studies (Silverton, Colorado), established two energy balance and detailed radiation towers in the Senator Beck Basin Study Area (SBBSA). The SBBSA is a research catchment in the headwaters of the Uncompahgre River of the Upper Colorado River Basin and is maintained and sampled by the Center for Snow and Avalanche Studies.

[7] The instrumentation on the towers was specifically designed and configured to facilitate energy balance modeling of the snowpack and assess the relative impacts of radiative forcing by dust, climate change, and climate variability. Along with energy balance data from a sibling tower on the Grand Mesa, Colorado (installed in the Fall of 2009), these are the only comprehensive energy balance and detailed radiation data for snow in the Upper Colorado River Basin. As such, they uniquely allow us to answer the question of how much does radiative forcing by dust deposition impact the energy balance and snowmelt of the mountain snowpack. In this paper, we present 6 years of dust loading data, meteorology, and detailed radiation data from the SBBSA. In the partner paper [*Skiles et al.*, 2012], we present the retrievals of dust radiative forcing in snow and investigate the impacts of that forcing and atmospheric warming on the acceleration of snowmelt.

2. Background

[8] Melting energy for mountain snow (in all but closed-canopy forest environments) comes primarily from net solar radiation, itself controlled by changes in irradiance and snow albedo [*Oerlemans*, 2000; *Bales et al.*, 2006; *Painter et al.*, 2007]. Snow albedo is controlled by changes in snow grain size (described by either optical grain size or specific surface area) and by light absorbing impurities such as dust, black carbon, and tree litter. Snow grain growth decreases snow albedo in the near-infrared (0.7 to 1.5 μm) and shortwave-infrared wavelengths (1.5 to 3.0 μm) whereas the light-absorbing impurities generally decrease the spectral albedo in the visible wavelengths (0.4 to 0.7 μm) (Figure 1).

[9] The spectral albedo of clean snow has values greater than 0.95 in the visible wavelengths but can drop to near 0.0 in the shortwave infrared wavelengths. Increases in grain size decrease the spectral albedo primarily in the range from 0.7 to 1.5 μm. These changes drive the decrease in broadband albedo for clean snow. However, absorbing impurities such as dust and carbonaceous particles decrease the spectral albedo in the visible wavelengths, from 0.95–0.98 down to as low as 0.30. Together, grain growth and absorbing impurities arguably give snow the greatest range of albedo of any surface on Earth.

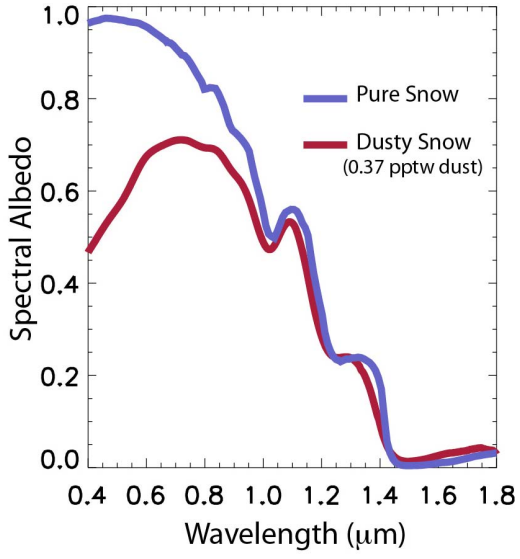

Figure 1. Spectral albedo of clean snow (modeled) and snow with dust concentration of 0.37 parts per thousand by weight of snow water or mg g^{-1} (measured).

[10] The dust and carbonaceous particles are heated by absorption of solar radiation and, in turn, they heat the surrounding snow primarily through conduction to the contiguous snow grains. Once the surrounding snow is at 0°C, the additional radiative forcing contributes to melting of those grains. Timing of deposition of impurities and persistence at or near the snow surface determines their influence on snowmelt. Dust that is deposited during midwinter events is usually buried by subsequent snow accumulation, limiting the amount of time it spends at or near the snow surface absorbing solar radiation. Importantly, the particle size of dust is generally large enough that it is not entrained in snowmelt and washed to deeper layers away from its radiative forcing capacity [*Higuchi and Nagoshi*, 1977; *Conway et al.*, 1996]. Instead, the dust remains in its layer while overlying snow melts and percolates to below the dust. As overlying dust layers merge with those previously buried, the visible spectral albedo decreases further, increasing radiative forcing and snowmelt. Spring often brings further dust events, which accelerate snowmelt through their direct reduction of albedo, and further reduce snow albedo by accelerating the growth of snow grains.

3. Study Area, Instrumentation, and Observations

[11] We present data from two micrometeorological stations measuring energy balance and radiation fluxes in the

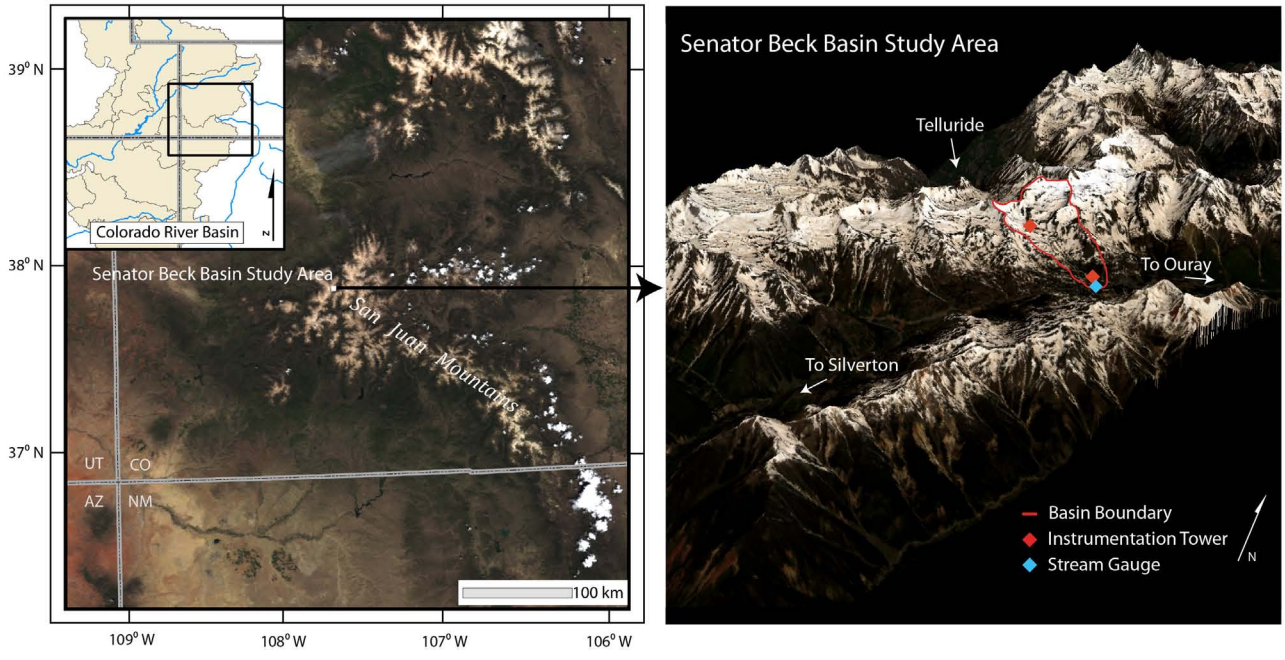

Figure 2. Overview of the Senator Beck Basin Study Area. The Swamp Angel Study Plot and Senator Beck Study Plot are indicated.

Senator Beck Basin Study Area (SBBSA), western San Juan Mountains in the Upper Colorado River Basin (37° 54′ 30″ N, 107° 43′ 30″ W) (Figure 2). The SBBSA lies in a generally east-facing basin with the stations in the alpine and the subalpine. As the first two complete energy balance and detailed radiation stations in the Upper Colorado River Basin, they uniquely generate knowledge of snowmelt dynamics in that region. In 2009, we added a similarly instrumented tower on the Grand Mesa of Colorado, ∼150 km to the north.

[12] The alpine site, Senator Beck Study Plot (SBSP), sits on level tundra at 3719 m with a 10 m instrument tower and a 12 m by 36 m snow profile plot in which snow properties and dust concentrations are observed regularly (Figure 3a). The site is exposed to strong winds and its measurements are considered representative of a wind-affected snow cover setting.

[13] The subalpine Swamp Angel Study Plot (SASP) is located in a wind-protected forest clearing at 3368 m (Figure 3b). Wind speeds are much lower than at the alpine site and wind redistribution of snow cover is negligible. The study site contains a 30 m × 30 m snow profile plot, a storage precipitation gauge, and a 6 m tower holding the same instrumentation array as on the SBSP tower. The Senator Beck Stream Gauge (SBSG) is located about 100 m downstream of the subalpine tower at the basin outlet.

[14] The towers are instrumented with up- and down-looking broadband solar and filtered near-infrared/shortwave-infrared pyranometers (Kipp&Zonen CM21 and Kipp&Zonen CM21 with Schott RG695 glass filters), up-looking longwave pyrgeometers (Kipp&Zonen CG4), and down-looking surface temperature sensor for estimating snow-emitted longwave radiation (AlpuG GmbH SnowSurf). Wind speed, wind direction, air temperature, and relative humidity are measured every 5 s at two heights (RM Young™ model 05,103-5 and Campbell Scientific™ CS500). Snowpack depth at both towers is measured at the end of each hour by an ultrasonic distance sensor (Campbell Scientific™ SR50).

[15] Precipitation (mm) is measured at the subalpine site in an open topped collector; accumulated fluid is weighed every 5 s and reported hourly. Precipitation is not measured at the alpine site because of frequent high winds that would under sample snowfall. All subhour measurements are averaged hourly and daily. A hexagonal array of vertical 3 m snow depth measurement stakes are deployed around the tower at a radius of 7.5 m to calculate the snow surface gradient to allow correction of incident radiation measured by the level up-looking pyranometers and in turn the calculation of albedo (Table 1).

[16] Dust loading and dust concentrations are sampled within the alpine and subalpine snow study plots for each dust event. We sample dust layers, as soon after deposition as site access is possible and safe from avalanches. The dust loading is determined by collecting the dust layer and some clean snow above and below the layer in a column over a 0.5 m^2 area. These samples are melted, dried, and preserved, and single event dust mass flux is recorded (g m^{-2}). For each event, an additional bulk sample of dust mass (sample size dependent on volume of observer's backpack) is collected for texture and chemical analysis. The Earth Surface Processes Laboratory of the United States Geological Survey, Colorado, performs the texture and chemical analyses. The results from these analyses have been presented in the work of *Lawrence et al.* [2010]. These analyses reveal that dust deposited here is composed of primarily silt- and clay-sized particles, consistent with the observations that the dust sources are regional. The dust has composition of 8% organics and 92% mineral matter, with enrichments of heavy metals including As, Cu, Cd, Mo, Pb, and Zn.

[17] Regular sampling of snow pits within the study plot boundaries is used to monitor the thermal and metamorphic

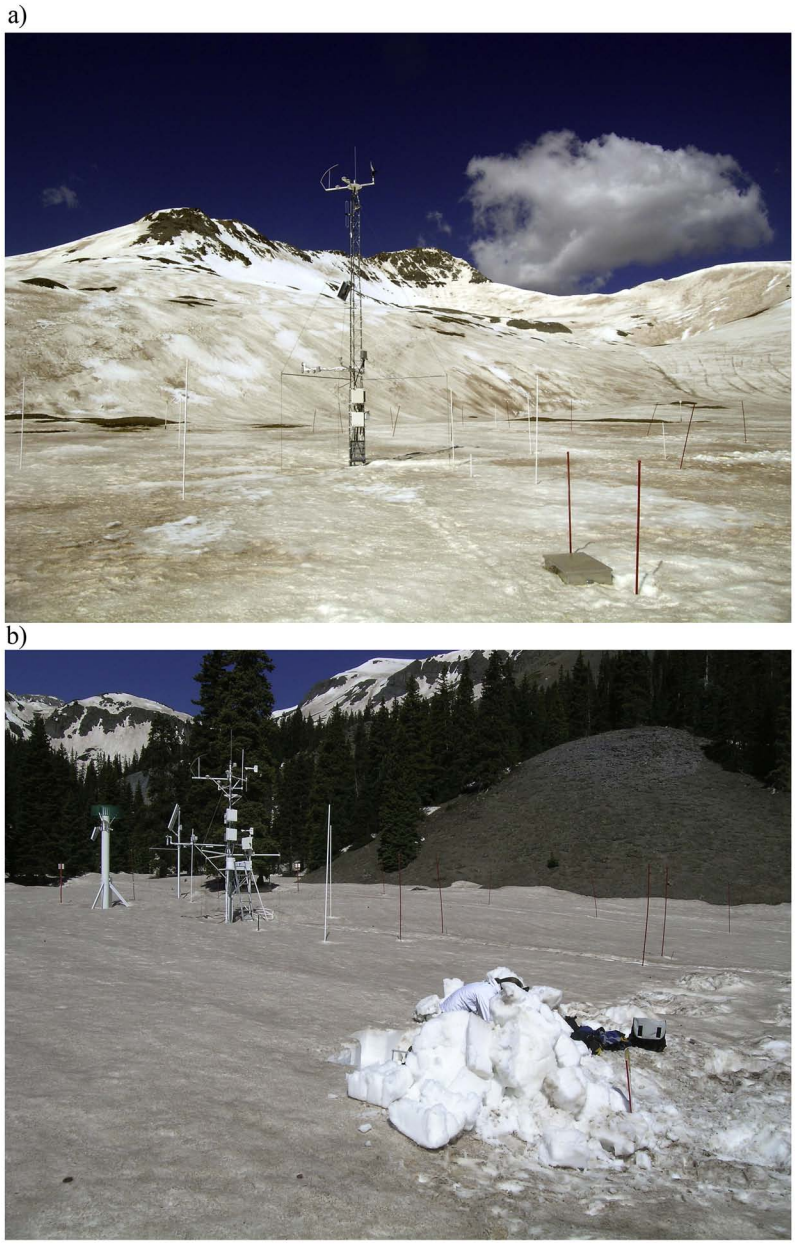

Figure 3. Energy balance/radiation towers. (a) Senator Beck Study Plot (alpine site), 12 May 2009. (b) Swamp Angel Study Plot (subalpine site), 13 May 2009.

state of the snowpack and layering of dust concentration. Pits are sampled monthly during the winter and weekly during the ablation season, with specific timing of observations subject to avalanche conditions. Weekly sampling generally starts in mid-March. In order to understand the relationship between snow albedo at the meteorological stations and dust concentration in the near surface layers of the snowpack, we collect the top 30 cm of the snowpack at

Table 1. Energy Balance and Radiation Measurements

Measurement/Instrument/Range	Subalpine	Alpine
Up/down broadband shortwave fluxes; Kipp&Zonen CM21 pyranometer; 0.285–2.800 μm	•	•
Up/down filtered shortwave fluxes; Kipp&Zonen CM21 pyranometer w/RG695 glass; 0.695–2.800 μm	•	•
Longwave irradiance; Kipp&Zonen CG4 pyrgeometer; 4.500–42.000 μm	•	•
Snow surface temperature; AlpuG GmbH SnowSurf	•	•
Air temperature and relative humidity; Campbell/Vaisala CS500-U (2 heights)	•	•
Wind speed and direction; RM Young 05,103-5 (2 heights)	•	•
Barometric Pressure; Campbell/Vaisala PTB101B (CS105)	•	•
Precipitation; ETI Instrument Systems Noah II	•	

3 cm intervals with horizontal area of 500 cm^2 (Figure 4), 30 cm being the nominal limit of shortwave radiation penetration into the snowpack. These 3 cm $\times$ 500 cm^2 snow samples are melted and filtered with individually preweighed 0.495 μm Nuclepore pore diameter filters. With the differential dust mass and the total snow sample mass, we report the dust concentration in milligram of dust per gram of snow sample (mg g^{-1}). The last sampling of the season occurs just prior to snowpack depletion when dust from all events has generally converged at the surface (except perhaps those that may have occurred just at the beginning of snowfall). Because dust is generally not entrained in melt, we use these samples to report end of year dust concentration. To determine the total dust load for the snow cover period, we sum the dust masses across all layers of the last snow pit before complete melt and multiply the 0.05 m^2 area by 20 to report the column dust load in grams per meter squared (g m^{-2}). This method is of course sensitive to spatial variability and this sensitivity motivates emerging remote sensing technology that will allow us to determine the spatial variation in dust radiative forcing and refined estimates of total loading.

[18] Given that the gradient of the snow surface beneath the down-looking pyranometers changes by snow accumulation, wind redistribution and heterogeneous snowmelt, calculations of snow albedo with the uncorrected radiation flux measurements (i.e., assuming a level snow surface) can be erroneous. The up- and down-looking pyranometers are both estimated to be level to within 1°, given design and installation. Therefore, the up-looking pyranometer measures the hemispherical irradiance onto a level surface. The direct ratio of the reflected flux with the irradiance measurement for albedo assumes that the down-looking pyranometer measures flux from a level surface. However, the snow surfaces at the subalpine and alpine towers are never level while snow covered (Figure 5) and therefore, the uncorrected ratio for albedo introduces a severe asymmetric artifact to the diurnal cycle of albedo (Figure 6). *Jonsell et al.* [2003] give an excellent description of this effect and the asymmetries of albedo calculations.

[19] We determine the slope and aspect of the snow surface with an array of graduated snow stakes that are referenced to an origin at the ground surface immediately beneath the down-looking broadband pyranometer and the sonic snow depth sensor. At the subalpine tower we have 4 stakes and the sonic depth sensor for a total of 5 measurements. Because of the stronger wind redistribution and variability of snow surface slope and aspect at the alpine tower (Figure 5), we have 6 stakes and the sonic depth sensor for a total of 7 measurements. On a weekly basis, a Center for Snow and Avalanche Studies observer visits each site and notes the snow depth at each stake, and snow depth is recorded on an hourly basis with the sonic depth sensor. The time series of snow depths at each stake and each sonic depth sensor is interpolated linearly between each measurement to a daily time step. For each day, we then determine

Figure 4. Snowpit sampling for stratigraphy of dust concentration, 7 May 2009.

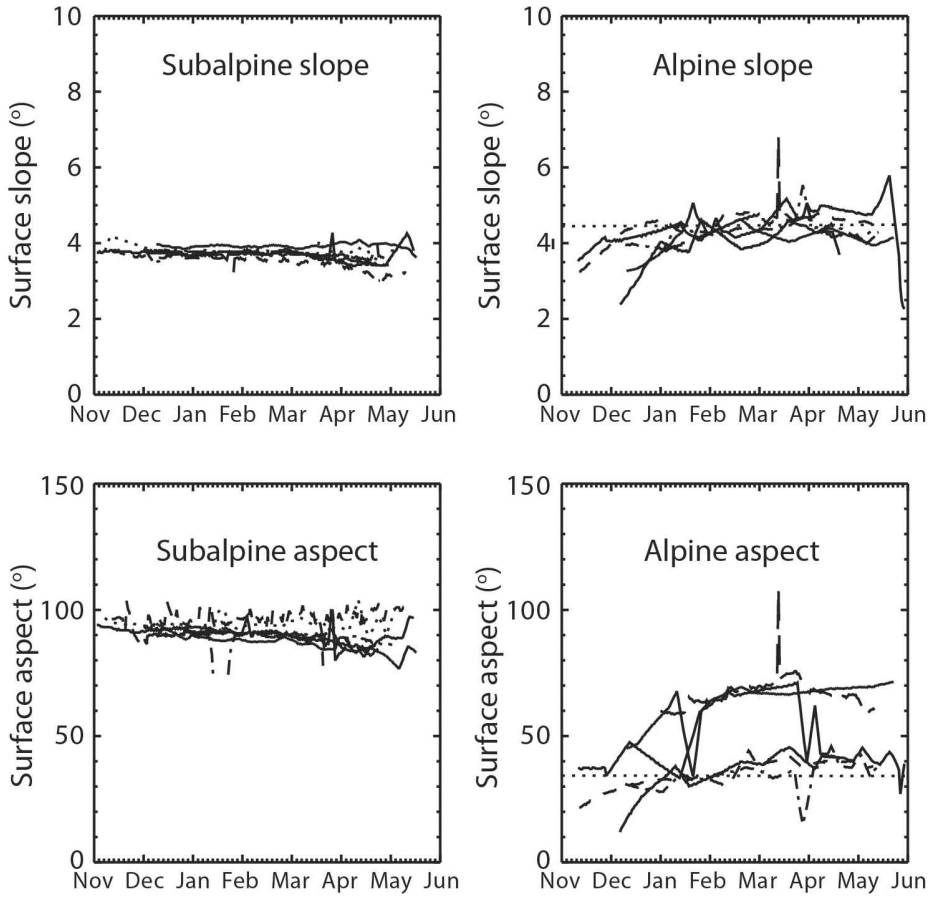

Figure 5. Time series of snow surface geometry for all years in 2005–2010. (a) Subalpine slope. (b) Alpine slope. (c) Subalpine aspect. (d) Alpine aspect. Aspect referenced clockwise from north, such that east is 90° and west is 270°.

the best fit of a plane to the snow depth arrays. The gradient of this plane gives the surface to which we correct the broadband and NIR/SWIR irradiances. We then correct albedo according to the following relationships (Figure 6):

$$\cos\beta = \cos\theta_s \cos\theta_n + \sin\theta_s \sin\theta_n \cos\{\phi_s - \phi_n\}, \qquad (1)$$

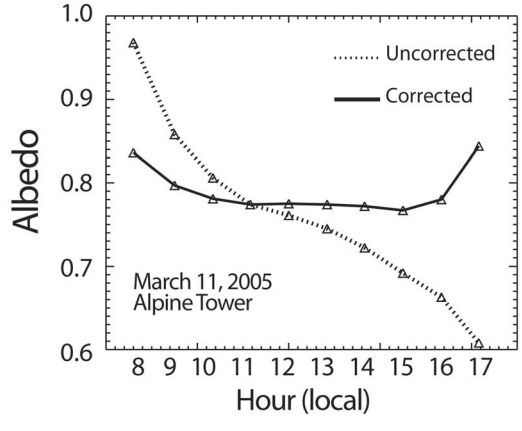

Figure 6. Correction of diurnal variation in snow albedo at the alpine site, using the slope and aspect data in Figure 5.

where β is the local solar zenith angle, θ_s is the solar zenith angle for a horizontal surface, ϕ_s is the solar azimuth angle, θ_n is the surface slope, and ϕ_n is the surface aspect. The scalar by which we correct the measured downward irradiances to at-surface irradiances is given by

$$M_\beta = \frac{\cos(\beta)}{\cos(\theta_s)}. \qquad (2)$$

The direct proportion of the surface irradiance, the proportion of the total irradiance as determined from modeling of the potential irradiance with the Santa Barbara DISORT Atmospheric Radiative Transfer (SBDART), is scaled by M_β and added back to the diffuse irradiance. We assume that the diffuse irradiance is relatively unchanged with slope and aspect. This assumption is being tested in other work but the correction of albedos suggests that it is valid.

[20] Wind speeds are markedly lower at the subalpine site. When snow accumulates on the up-looking pyranometers, it occludes the irradiance from the pyranometer. The sensor then reports irradiances that are often lower than the reflected fluxes. When this is the case, we correct these irradiances by assuming that the albedo at the subalpine site ($\alpha_{subalpine}$) is the same as at the alpine site (α_{alpine}). The basis for this assumption is that snow occlusion of the

up-looking pyranometers occurs when fresh snowfall has occurred. Our observations indicate that the albedos of new snow at the subalpine and alpine lie within 2% of each other without bias. Therefore, we back-calculate the subalpine broadband irradiance, $S_{subalpine}$, as follows:

$$S_{subalpine} = \frac{K_{subalpine,reflected}}{\alpha_{alpine}}, \quad (3)$$

where $K_{subalpine,\ reflected}$ is the measured reflected flux.

[21] We also measure aerosol optical depth and other atmospheric column properties at the subalpine site with a CIMEL sunphotometer. This sunphotometer has operated in the NASA Aerosol Robotic Network (AERONET) since the autumn of 2005 with modest interruptions. The site name is Red_Mountain_Pass and can be found on the AERONET website at http://aeronet.gsfc.nasa.gov/new_web/photo_db/Red_Mountain_Pass.html. The measurements from the Red_Mountain_Pass AERONET site will be described in a subsequent paper due to the complexity of these data.

4. Results

[22] We present the timing of dust deposition events, time series of concentrations, and the meteorological and energy balance results. Part 2 of this paper [*Skiles et al.*, 2012] presents the radiative forcing and snowmelt modeling results.

4.1. Timing of Dust Deposition to Snow

[23] Figure 7a shows the timing of dust deposition events to snow cover in the SBBSA for years 2005 through 2010 during the winter through spring. A dust deposition event is defined as that which can be observed by the eye in the mountain snowpack. Annual distributions are generally centered in April but with some distinct clustering. Deposition events in 2006 and 2007 spanned four months from winter into spring until the end of snow cover whereas events in 2008 through 2010 only spanned two months. Moreover, 2009 and 2010 saw by far the greatest dust loading in these more compressed periods but with shifted spans of 27 February to 25 April and 30 March to 22 May.

[24] Figure 7b gives the summary distribution by month across all dust to snow deposition events. While a few events occur in the late autumn, most events occur after the desert regions have dried from winter snowfall and rain but synoptic scale storms continue to bring precipitation to the region. It is clear that, across this period of record, the vast majority of events occur during March–April–May (MAM), dominated by events in April. The majority of snowfall in the mountains of the Upper Colorado occurs before the MAM period. Therefore, the timing of the majority of dust events is such that they remain closer to or at the snow-atmosphere interface where their radiative forcing and efficacy in accelerating snowmelt is maximized. Snow cover exists in the SBBSA generally from October through mid June.

4.2. Dust Concentrations

[25] Dust loading is partly driven by the number of dust events in a snow season, but the magnitude of dust loading is highly variable annually (Figure 8). It is near-snow surface dust concentration that governs the albedo reduction

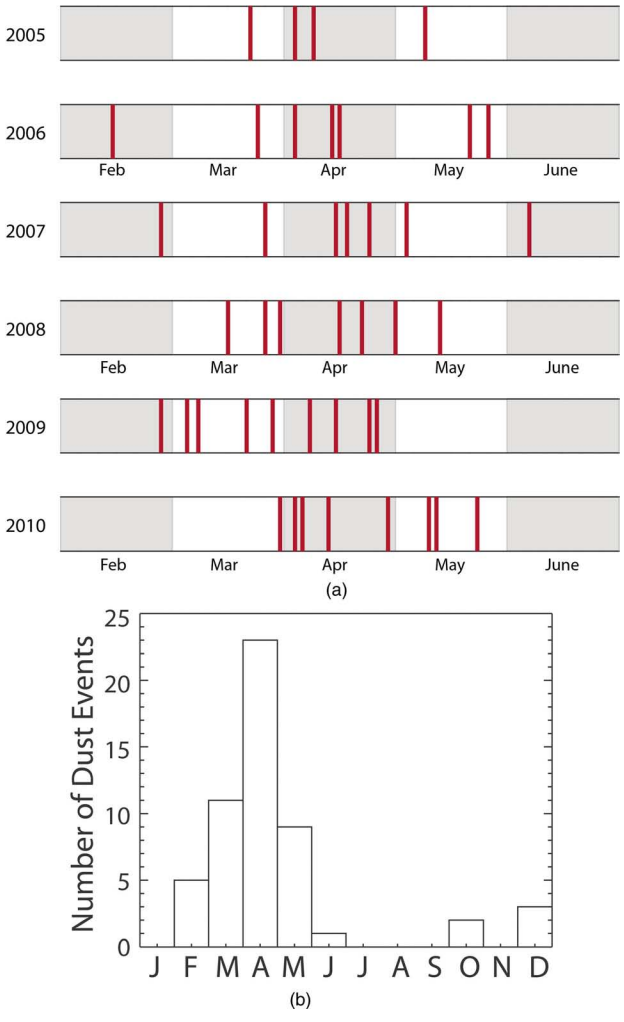

Figure 7. (a) Annual distributions of dust deposition events to snow cover in SBBSA across 2005 through 2010. (b) Histogram of dust deposition events in SBBSA across 2005 through 2010.

and radiative forcing, and as such the number of dust events is not necessarily a good predictor of end-of-year snow albedo or of dust radiative forcing (Figure 8). While we know the various controls of dust emission, transport, and deposition in isolation, we are still in the infancy of understanding their relative contributions. We differentiate those events that occur after 1 March to highlight those events that can have the greater radiative and snowmelt impact (Figure 8a) due to the longer period over which these dust layers exist on the snow surface. The number of dust deposition events increased quasi-monotonically over the period of our study (since 2005) (Figure 8b), whereas dust loading has not. For example, 2008 and 2009 had the same number of dust events after 1 March, respectively, but the end of snow cover dust concentration in 2009 (4.16 mg g^{-1}) was about 6 times greater than in 2008 (0.71 mg g^{-1}). The greatest end of snow cover dust concentrations occurred in 2009 (4.16 mg g^{-1}) and 2010 (4.14 mg g^{-1}). These concentrations were nearly 5 times greater than that recorded in 2006 (0.86 mg g^{-1}), the third highest dust concentration year, and more than an order of magnitude

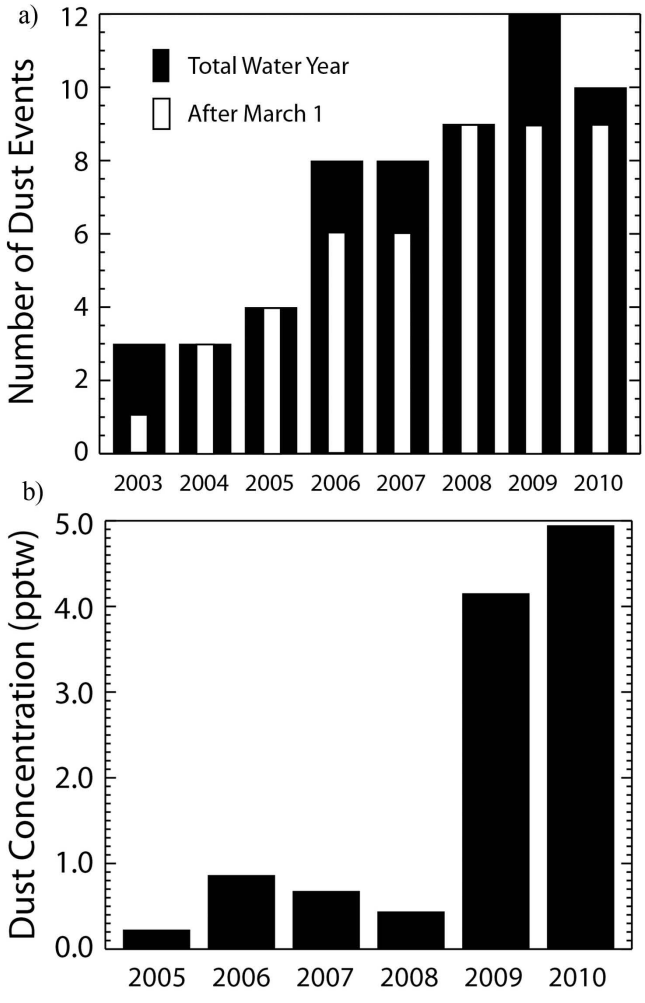

Figure 8. (a) Annual number of dust events in SBBSA in 2003–2010. (b) Annual end-of-melt season dust concentration in snowpack at the subalpine site and alpine site for 2005–2010.

greater than in 2005 (0.23 mg g^{-1}), the year with the least dust loading. Given the short period of record, it is not possible to determine whether the observed increase in dust events is part of a longer-term trend, a decadal-scale cycle, or an artifact of the observation period. As with the end of snow cover concentrations, the total dust loadings in 2009 and 2010 were by far the greatest (54.6 g m^{-2} and 45.6 g m^{-2}, respectively). In other years, dust loading ranged from 4.7 g m^{-2} to 12.7 g m^{-2}.

[26] The weekly sampling of the stratigraphy is presented as images in Figure 9 in which the vertical dimension gives the stratigraphy of the top 30 cm in 3 cm increments, and the horizontal dimension gives the approximately weekly time resolution. As noted previously, the dust concentrates on the snow surface as melt progresses, which is readily apparent in the stratigraphy time series. Spring snow events are evident, moving the high surface concentration lower in the top 30 cm layer. The increase in surface concentration with time correlates directly with the observed coincident reductions in snow surface albedo.

4.3. Meteorological and Energy Balance Measurements

[27] We show the daily meteorological data for the subalpine and alpine sites in Figure 10. Mean temperatures at the lower elevation subalpine site are most often slightly higher than those at the alpine site (Figure 10a). At the subalpine site, temperatures ranged from −24°C to 16°C with a mean annual temperature at the melting point of ice of 0°C. At the alpine site, temperatures ranged from −25°C to 15°C with a mean of −1°C.

[28] Daily mean relative humidity (RH) ranged generally from 20 to 95% with the rare excursion to as low as 10% (Figure 10b). Through most of the years, the time-integrated mean RH lies in the range 60 to 80% but begins to drop markedly in the period April/May to a minimum very near the summer solstice. At this point, the summer monsoon generally commences. The one exception to this pattern in this record was the spring of 2009 when the drying began but was quickly supplanted by a return to strong precipitation. The mean annual relative humidity at the subalpine site is 62% and for the alpine site is 58%, despite the higher temperatures at the subalpine site, possibly an effect of the surrounding forest. The difference between the two however lies within the 3% uncertainty for the RH instruments.

[29] The difference in wind speed is the most obvious difference between the meteorology at the alpine site and the subalpine site (Figure 10c). At the alpine site, the mean wind speeds were 3.7 m s^{-1} with a range of daily means of 1.1 to 11.1 m s^{-1}. At the subalpine site, the mean wind speeds were 1.1 m s^{-1} with a range of 0.3 to 3.7 m s^{-1}. Whereas wind speeds at the subalpine site have little sensitivity to season, wind at the alpine site has a strong seasonality with maximum wind speeds in winter and minimum wind speeds in July and August. The abrupt transition to lower wind speeds in summer coincides with the abrupt return of relative humidity to wintertime ranges.

[30] The global irradiance time series show that the SBBSA has relatively high irradiances due to less frequent cloud cover than in settings such as the Pacific Northwest, consistent with its characterization as a radiation-dominated continental climate (Figure 10d). Given its higher elevation and lower optical air mass, the alpine site irradiance is generally higher than that of the subalpine site. The alpine mean global irradiance was 217 W m^{-2} with a range of daily means of 43 to 424 W m^{-2}. The subalpine mean global irradiance was 205 W m^{-2} with a maximum of 403 W m^{-2}. The minima in the subalpine record are more uncertain because of the corrections described above when snow lies on the up-looking pyranometer. Whereas our calculations have minima <20 W m^{-2}, we are confident that the minimum mean global irradiances lie in the range of 35–45 W m^{-2}. The minima in the alpine record are more reliable because higher wind speeds prevent accumulation of snow or frost.

[31] The alpine site has generally higher reflected fluxes than the subalpine because of greater global irradiance (Figure 10e) but also because it maintains a higher albedo (Figure 11). Both sites exhibit minimum reflected fluxes in summertime when vegetation is exposed. When snow cover is present, the reflected fluxes have minima near the

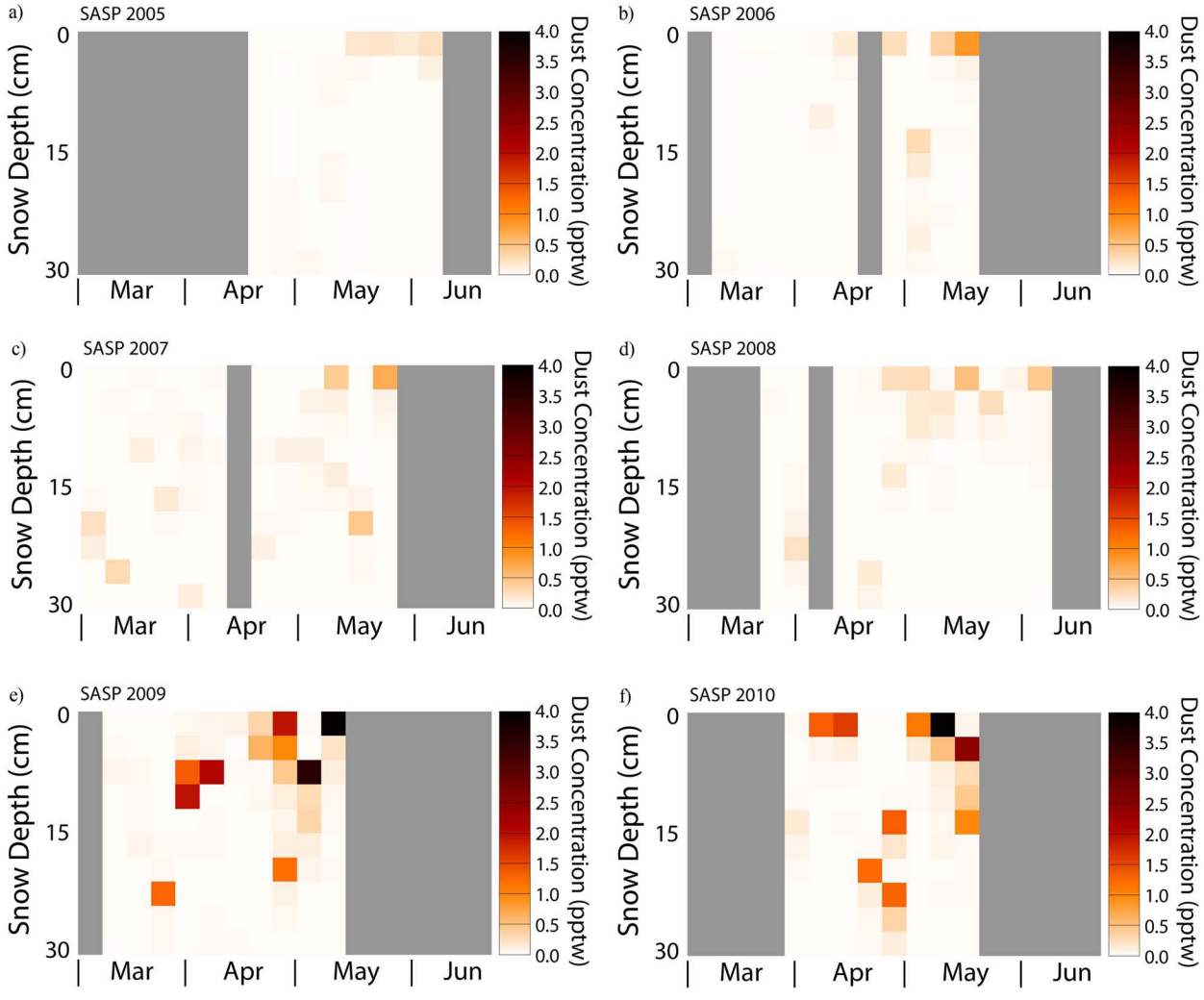

Figure 9. Image representation of the time series of dust concentrations in the top 30 cm of the snowpack at the subalpine Swamp Angel Study Plot (SASP) for 2005 through 2010. Gray columns indicate no data were collected. The continuous gray at the end indicate no snow remained.

winter solstice then rise with the global irradiance modulated by a relatively constant snow albedo until a peak that well precedes the loss of snow cover. It is during this later period that snow albedo drops due to dust radiative forcing and snow grain coarsening.

[32] Longwave irradiance is generally greater at the subalpine site due to higher temperatures, greater relative humidity, and greater air mass (Figure 10f). The larger contribution of terrain emission also increases the longwave irradiance at the subalpine site. Longwave irradiance abruptly increases in most years coincident with the increase in relative humidity and cloud cover near the summer solstice with the onset of the SW monsoon. At the subalpine site, the mean longwave irradiance was 250 W m^{-2} with minimum of 137 W m^{-2} and maximum of 344 W m^{-2}. At the alpine site, the mean longwave irradiance was 231 W m^{-2} with minimum of 118 W m^{-2} and maximum of 335 W m^{-2}. The climatology of each of these fields is presented in Figure 11.

[33] Declines in springtime broadband albedo (Figure 12) at the subalpine site generally precede those at alpine site by 1–2 weeks, due to greater wind-driven redistribution of dust into patchy exposure in the alpine and more frequent snowfall in the late spring in the alpine. The variation in albedo comes from periodic additions of new snow during both accumulation and melt, with especially large ranges (0.3–0.9) over short time intervals in the melt season as dust layers exert their strongest influence. The climatology of broadband albedo shows relatively stable albedo (0.8–0.85) at both sites until late March after which there is a quasi-monotonic decline until mid to late May (Figure 13). The subalpine albedo drops more rapidly than the alpine albedo. Slight plateaus of albedo occur in May at ~0.45 in the alpine and ~0.35 in the subalpine before plunging to the snow-free vegetation albedo of 0.15–0.20 in June.

[34] Figure 14 shows broadband, NIR/SWIR, and visible albedo over the ablation season (15 April to snow all gone date) for the subalpine site (Figures 14a, 14c, and 14e) and alpine site (Figures 14b, 14d, and 14f). The lowest end-of-year albedos occur in 2009, the year with the highest dust concentration, greatest radiative forcing, and earliest melt out date.

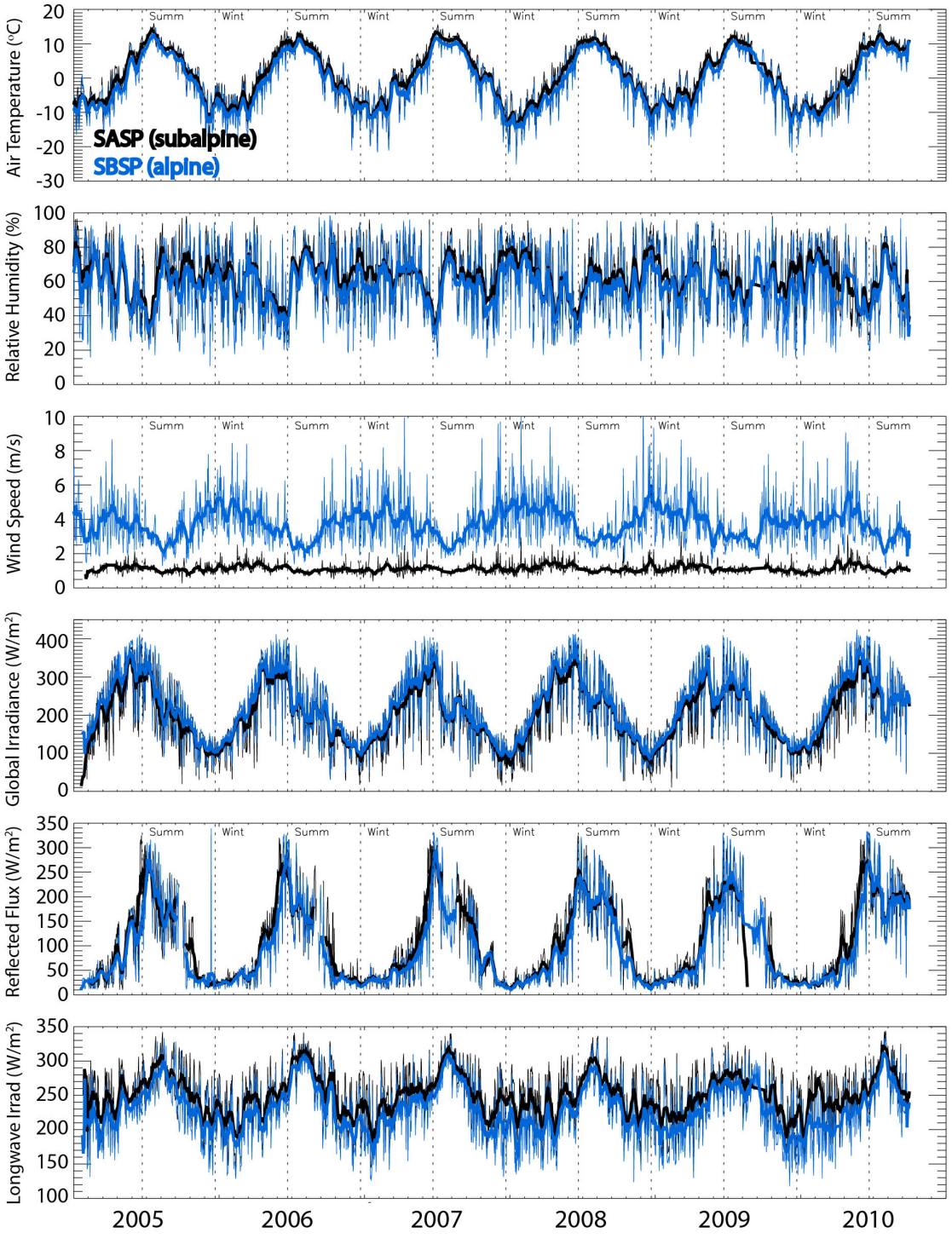

Figure 10. Time series of meteorological and radiation fields at subalpine and alpine sites for 2005 through 2010. The vertical dashed lines indicate the onset of winter (21 December) and summer (21 June). The global irradiance includes nighttime hours, so these are daily means. The year label in the abscissa axis is centered upon that calendar year's summer solstice.

[35] The decline in albedo happens relatively quickly in 2009 in comparison with the other years due to the greater radiative forcing driven by extremely high dust concentrations. There was a reduction in visible albedo from 0.72 to 0.33 over 13 days (day of year 109 to 121), more than doubling absorbed solar radiation. A precipitation event brought the albedo back up to 0.91 at day of year 122, but it dropped again to 0.33 within 5 days (day 127) and maintained a value of about 0.3 until melt out 11 days later (day 138). The lowest average albedo over the ablation season was also observed at the subalpine site at 0.49. At the alpine site there was a similar end of year decline in albedo, which was

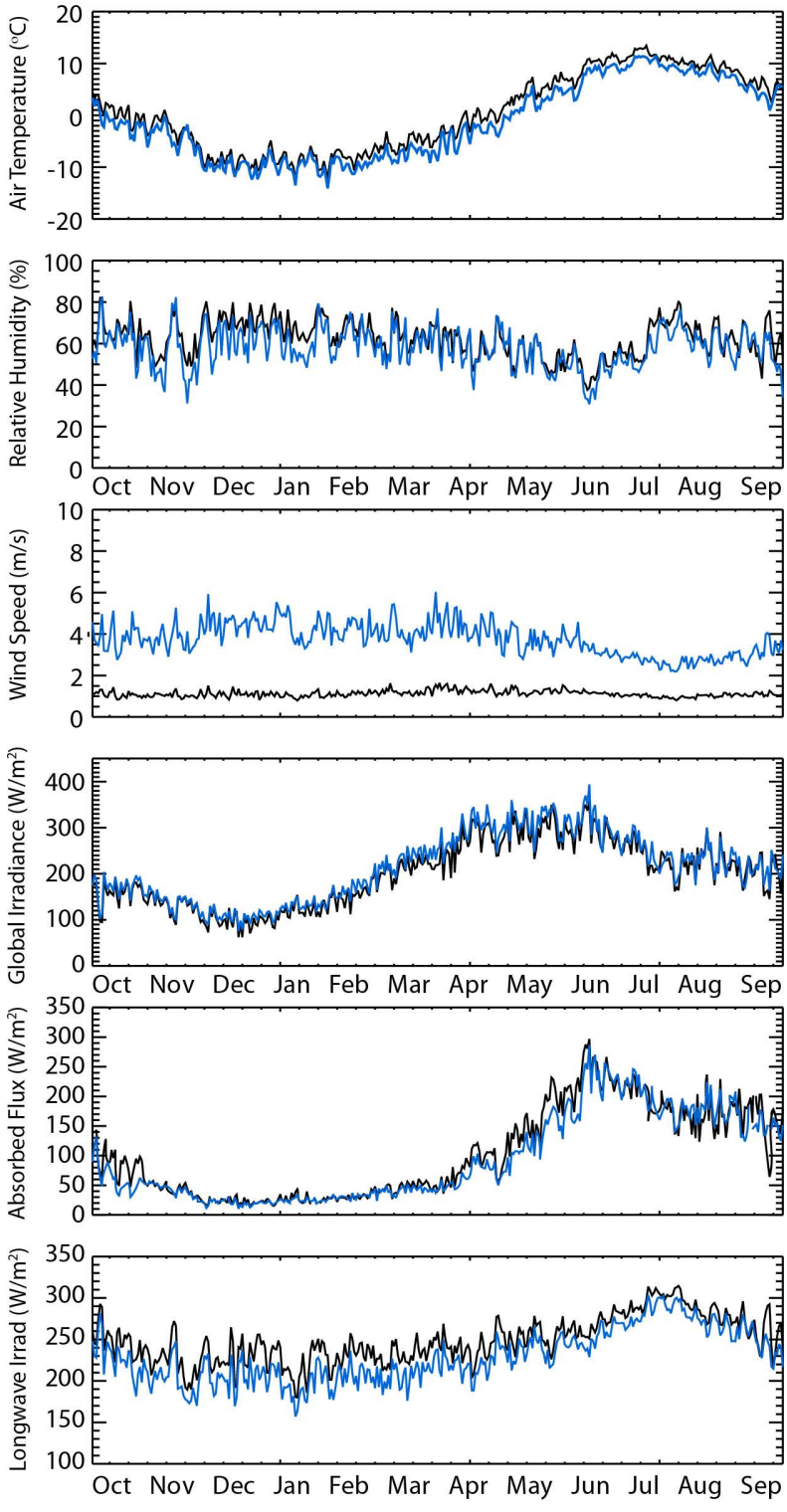

Figure 11. Daily climatologies across 2005–2010 of the meteorological and radiation fields given in Figure 10.

reduced from 0.9 at day 122 to 0.34 in 16 days (day 138) and melt out occurred within 2 days (day 140). Most literature cites snow albedo as ranging from 0.4–0.9, but 2009 and 2010 indicate values can be lower in the presence of heavy dust loading.

[36] Figure 15 shows daily snow depth and weekly snow water equivalent (SWE) for 2005 through 2010. As with other parameters, windier conditions at the alpine site cause redistribution of snow and therefore variable relationship between the snow depth measured by the sonic depth

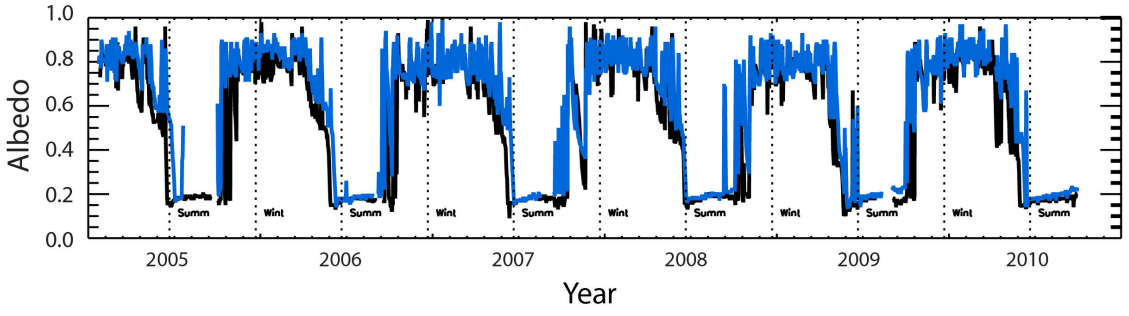

Figure 12. Time series of snow broadband albedo at subalpine and alpine sites for 2005 through 2010.

sensor on the tower and that measured in the snow pits a few meters away. However, the calmer conditions of the subalpine site allow consistency in measured snow depths at the subalpine tower and the snow pits.

[37] The magnitude of the impact of dust radiative forcing on changes in the date of snow all gone (SAG) depends on the timing and magnitude of snow accumulations before and after dust events and the total amount of snow on the ground over the melt season. For example, dust-forcing of melt of a snowpack consisting of 1 cm of SWE under average spring conditions would impact change in SAG by less than a day, whereas a 1 m snowpack allows a longer period of divergence between the dust-laden snow and a cleaner snow column subject to the same energy fluxes, resulting in multiple weeks of difference in SAG (as described in Part 2 of this paper).

[38] While there is interannual variability in snow depth and peak SWE, accumulation typically begins at the subalpine site between mid and late November and melts completely between mid May and mid June (Figure 16). Peak snow depth ranges from 2.1 m (2007) to 2.9 m (2008) with both a mean and median of 2.5 m. Peak tends to occur in mid April with the earliest peak being 27 March (2010) and latest 24 April (2007) with the mean on 11 April. At the alpine site, snow accumulation begins later (due to greater wind redistribution and scouring), typically in late November to early December, and persists between 1 day and 2 weeks later than the subalpine snowpack. Peak snow depth ranges from 1.7 m (2009) to 2.6 m (2005) with a mean of 2.1 m and a median of 2.0 m. Peak also occurs in mid April, with the earliest peak on 7 April (2006) and latest on 24 April (2010) with mean peak occurring on 15 April.

[39] Measured peak SWE at the subalpine site ranges from 682 mm (2010) to 977 mm (2008), with a mean of 798 mm and median of 776 mm and occurs on average on 22 April (Figure 15). At the subalpine site peak SWE ranges from 575 mm (2009) to 1019 mm (2005), with a mean of 764 mm and median of 748 mm and occurs on average on 27 April. Unlike snow depth, SWE is not measured continuously so these numbers may not represent actual peak SWE. Measured SWE peaks later than snow depth discussed above, as well as being slightly higher and later than at the nearby Red Mountain Snow Telemetry (SNOTEL) site where peak SWE occurs on average on 16 April with a mean SWE of 690 mm and median of 657 mm.

[40] Over the record, the subalpine site has on average a greater snow depth and SWE than the alpine site (Figure 16). In some years, such as 2008 and 2009, lower snow depth at the alpine relative to the subalpine site is more pronounced. While the alpine site always has consistently higher winds, these years also happen to be two of the windiest over the record; the enhanced winds in these years could be contributing to lower snow depths through redistribution and densification of the alpine snowpack. Due to the small spatial extent of our measurements and the high spatial heterogeneity of snow cover in alpine environments, we consider these snow depth and SWE measurements to be representative of our sites but not necessarily the landscape.

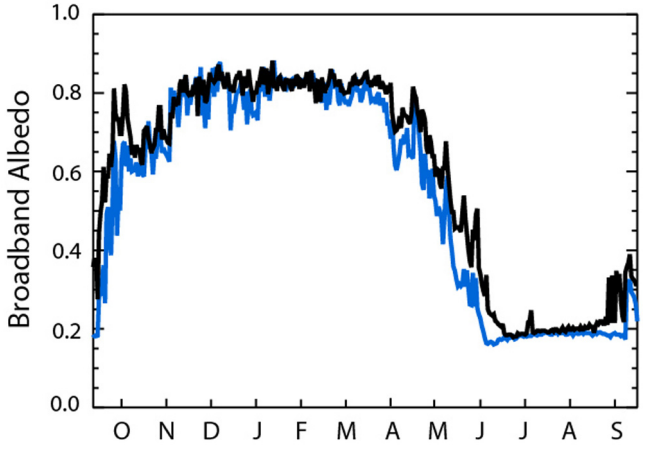

Figure 13. Daily climatology of snow albedo across 2005–2010 at subalpine and alpine sites.

5. Concluding Remarks

[41] The measurements described above are critical and unique in the Colorado River Basin. They have provided surprising insights into the controls on snowmelt and runoff in the CRB and will continue to enable monitoring and simulation of snowmelt forcings that exhibit strong interannual variability and are not captured by conventional or operational temperature index-based snowmelt models. *Painter et al.* [2007, 2010] demonstrate that dust radiative forcing of snowmelt has dramatic impacts on snowmelt timing, melt-out date, and hydrology across the Upper Colorado River Basin, with important ramifications for water management, planning, and policy.

[42] *Munson et al.* [2011] suggest that dust deposition on Colorado River snow stands to increase with regional warming. Therefore, it is possible that the heavy dust

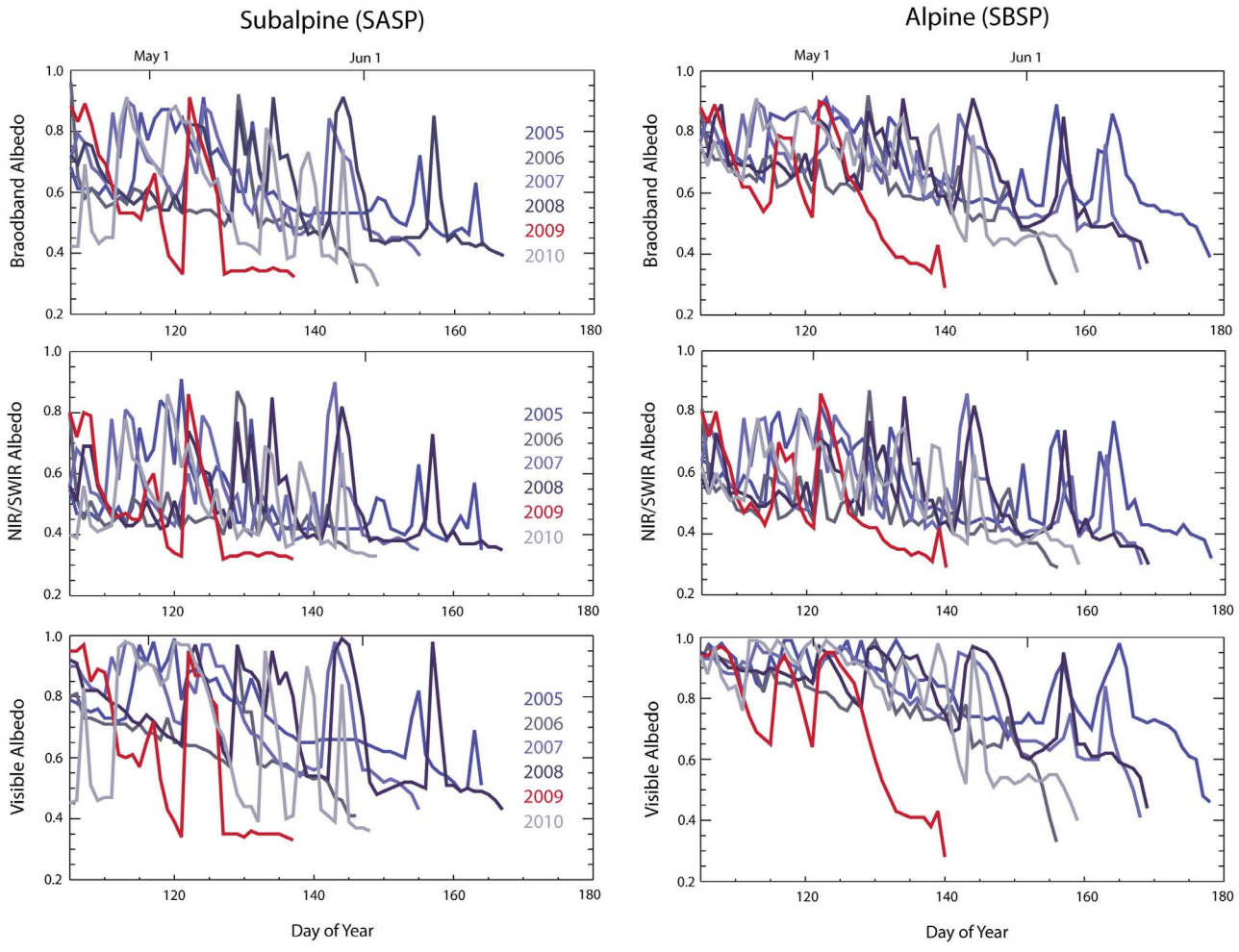

Figure 14. Time series of snowmelt season broadband, near-infrared/shortwave infrared (NIR/SWIR), and visible albedo by year for 2005–2010.

depositions observed in 2009 and 2010 represent the future normal condition. Many studies indicate that climate warming will strongly impact Colorado River flows [*Christensen and Lettenmaier*, 2007; *Barnett and Pierce*, 2009; *Hurkmans et al.*, 2009], as temperature increases change rain/snow proportions, the length of the snow season, and potential evapotranspiration. Recent bark beetle epidemics and associated forest management responses threaten to alter the hydrologic response of headwater catchments to diurnal and seasonal snowmelt cycles.

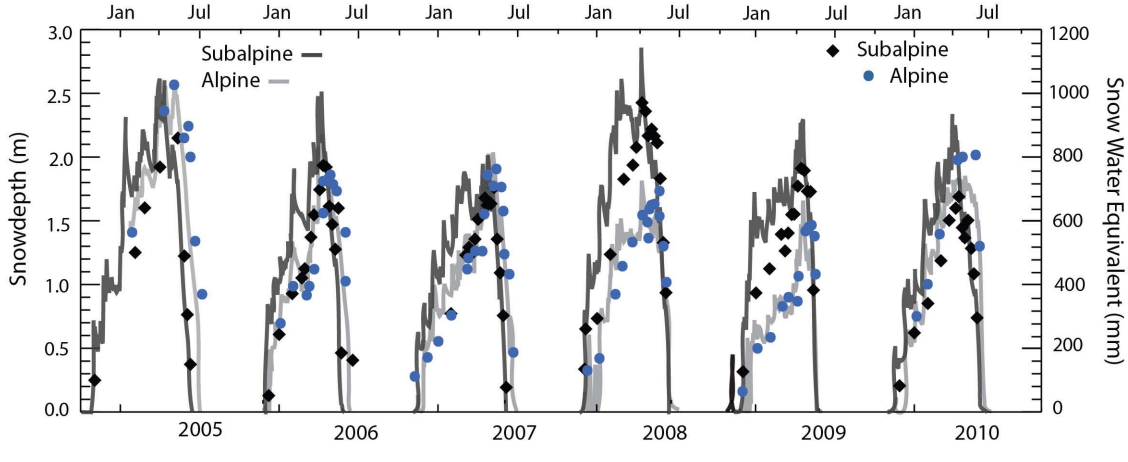

Figure 15. Time series of snow depth and snow water equivalent by year for 2005–2010.

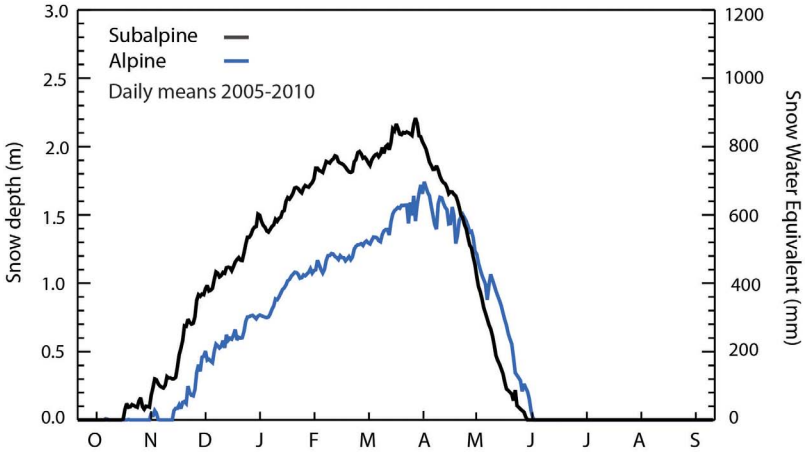

Figure 16. Daily climatology of snow depth across 2005–2010. We do not include climatology of SWE because of the sparse and out-of-phase nature of sampling.

[43] Analyses of snow accumulation and melt forcing under dust, climate warming, or vegetation change scenarios are not possible without the type of measurements detailed here—in fact, the far-reaching ramifications of the measurements and results described above, in the companion paper, and in the reference for *Painter et al.* [2007, 2010] demand an expanded capacity to conduct direct monitoring of snow energy balance throughout the Upper Colorado River Basin and other snowmelt-dominated basins in the Western United States.

[44] **Acknowledgments.** This work was funded by the National Science Foundation grants ATM04323237 and ATM0431955, and NASA project NNX10AO97G. We acknowledge the assistance of Andrew Barrett in data processing. Part of this work was performed at the Jet Propulsion Laboratory, California Institute of Technology under a contract with NASA. We thank Jeff Dozier, Steve Warren, and an anonymous reviewer for their suggestions that improved this manuscript.

References

Ajai, L., et al. (2011), *Fate of Mountain Glaciers in the Anthropocene*, 15 pp., Pontifical Acad. of Sci., Vatican City.

Bales, R. C., N. P. Molotch, T. H. Painter, M. D. Dettinger, R. Rice, and J. Dozier (2006), Mountain hydrology of the Western United States, *Water Resour. Res.*, *42*, W08432, doi:10.1029/2005WR004387.

Barnett, T. P., and D. W. Pierce (2009), Sustainable water deliveries from the Colorado River in a changing climate, *Proc. Natl. Acad. Sci. U. S. A.*, *106*, 7334–7338, doi:10.1073/pnas.0812762106.

Christensen, N. S., and D. P. Lettenmaier (2007), A multimodel ensemble approach to assessment of climate change impacts on the hydrology and water resources of the Colorado River Basin, *Hydrol. Earth Syst. Sci.*, *11*, 1417–1434, doi:10.5194/hess-11-1417-2007.

Conway, H., A. Gades, and C. F. Raymond (1996), Albedo of dirty snow during conditions of melt, *Water Resour. Res.*, *32*, 1713–1718, doi:10.1029/96WR00712.

Higuchi, K., and A. Nagoshi (1977), Effect of particulate matter in surface snow layers on the albedo of perennial snow patches, in *Isotopes and Impurities in Snow and Ice*, edited by J. F. Nye, F. Miller and H. Oeschger, IAHS AISH Publ., 118, 95–97.

Hurkmans, R., P. A. Troch, R. Uijlenhoet, P. Torfs, and M. Durcik (2009), Effects of climate variability on water storage in the Colorado River Basin, *J. Hydrometeorol.*, *10*, 1257–1270, doi:10.1175/2009JHM1133.1.

Jonsell, U., R. Hock, and B. Holmgren (2003), Spatial and temporal variations in albedo on Storglaciaren, Sweden, *J. Glaciol.*, *49*, 59–68, doi:10.3189/172756503781830980.

Kaspari, S., P. A. Mayewski, M. Handley, S. Kang, S. Hou, S. Sneed, K. Maasch, and D. Qin (2009), A high-resolution record of atmospheric dust composition and variability since A.D. 1650 from a Mount Everest ice core, *J. Clim.*, *22*, 3910–3925, doi:10.1175/2009JCLI2518.1.

Lawrence, C. R., T. H. Painter, and J. C. Neff (2010), Contemporary geochemical composition and flux of aeolian dust to the San Juan Mountains, Colorado, United States, *J. Geophys. Res.*, *115*, G03007, doi:10.1029/2009JG001077.

MacDonald, G. M. (2010), Water, climate change, and sustainability in the southwest, *Proc. Natl. Acad. Sci. U. S. A.*, *107*, 21,256–21,262, doi:10.1072/pnas.0909651107.

Munson, S. M., J. Belnap, and G. S. Okin (2011), Responses of wind erosion to climate-induced vegetation changes on the Colorado Plateau, *Proc. Natl. Acad. Sci. U. S. A.*, *108*, 3854–3859, doi:10.1073/pnas.1014947108.

Neff, J. C., A. P. Ballantyne, G. L. Farmer, N. M. Mahowald, J. L. Conroy, C. C. Landry, J. T. Overpeck, T. H. Painter, C. R. Lawrence, and R. L. Reynolds (2008), Increasing eolian dust deposition in the western United States linked to human activity, *Nat. Geosci.*, *1*, 189–195, doi:10.1038/ngeo133.

Oerlemans, J. (2000), Analysis of a 3 year meteorological record from the ablation zone of Morteratschgletscher, Switzerland: Energy and mass balance, *J. Glaciol.*, *46*, 571–579, doi:10.3189/172756500781832657.

Painter, T. H., A. P. Barrett, C. C. Landry, J. C. Neff, M. P. Cassidy, C. R. Lawrence, K. E. McBride, and G. L. Farmer (2007), Impact of disturbed desert soils on duration of mountain snow cover, *Geophys. Res. Lett.*, *34*, L12502, doi:10.1029/2007GL030284.

Painter, T. H., J. S. Deems, J. Belnap, A. F. Hamlet, C. C. Landry, and B. Udall (2010), Response of Colorado River runoff to dust radiative forcing in snow, *Proc. Natl. Acad. Sci. U. S. A.*, *107*, 17,125–17,130, doi:10.1073/pnas.0913139107.

Ramanathan, V., M. V. Ramana, G. Roberts, D. Kim, C. Corrigan, C. Chung, and D. Winker (2007), Warming trends in Asia amplified by brown cloud solar absorption, *Nature*, *448*, 575–578, doi:10.1038/nature06019.

Skiles, S. M., T. H. Painter, J. S. Deems, A. C. Bryant, and C. Landry (2012), Dust radiative forcing in snow of the Upper Colorado River Basin: Part II. Interannual variability in radiative forcing and snowmelt rates, *Water Resour. Res.*, doi:10.1029/2012WR011986, in press.

United Nations Environmental Programme/World Meteorological Organization (2011), *Integrated assessment of black carbon and tropospheric ozone*, 285 pp., U. N. Environ. Prog., Nairobi, Kenya.